Phys Chem Minerals (2001) 28: 322–331

ORIGINAL PAPER

C. I. Sainz-Diaz · A. Hernández-Laguna · M. T. Dove

Theoretical modelling of *cis*-vacant and *trans*-vacant configurations in the octahedral sheet of illites and smectites

Received: 4 September 2000 / Accepted: 29 January 2001

Abstract The *cis*-vacant configurations of smectites and illites have been studied theoretically by using transferable empirical interatomic potentials. A wide range of compositions of octahedral and tetrahedral cation and interlayer charge has been considered. All results have been compared with the *trans*-vacant configurations in each sample. The calculated values reproduce the differences in the lattice parameters between the *cis*- and *trans*-vacant configurations of experimental studies. Taking into account the *cis*-/*trans*-vacant proportion, the calculated structures agree with experiment for the main structural features of the crystal lattice. The effect of the cation substitution in the octahedral and tetrahedral sheets on the cell parameters has been also studied, finding good linear relationships. The calculated cation substitution effects are consistent with experimental results. Although the energy difference between the *cis*- and *trans*-vacant configurations is small, the *cis*-vacant is more stable when the composition of clays is more smectitic, like the experimental behaviour. Similar trends of the cation substitution effect on the *cis*-/*trans*-vacant proportion to the experimental results are found. The structure of the hydroxy groups has also been analysed. The OH bond length, the orientation of the O–H bond with respect to the (001) plane and the non-bonding H...O distances have been studied.

Key words *Cis*-, *trans*-vacant configurations · Smectite · Illite · H-atom positions · Cation substitution effect

C. I. Sainz-Díaz (✉) · A. Hernández-Laguna
Department of Earth Sciences and Environmental Chemistry,
Estación Experimental del Zaidín, CSIC,
Profesor Albareda 1, 18008 Granada, Spain
e-mail: sainz@eez.csic.es

M. T. Dove
Department of Earth Sciences,
University of Cambridge,
Downing Street,
Cambridge CB2 3EQ UK

Introduction

Clay minerals have a layer structure where two tetrahedral layers sandwich a sheet of octahedrally coordinated cations. These minerals have a wide range of chemical composition and different isomorphous cation substitutions in the octahedral and tetrahedral sheets. In dioctahedral clays, isomorphous substitution of Al^{3+} by Mg^{2+} in the octahedral sheet, or Si^{4+} by Al^{3+} in the tetrahedral sheet, results in a net negative charge. This charge is compensated by the presence of additional cations in the interlayer space. Cation substitutions in octahedral and tetrahedral sheets create disordering phenomena in the crystal lattice structure of these minerals. Besides, the geometrical similarity of these layer silicate structures facilitates the formation of structures containing different kinds of layers and different ordered and disordered sequences of layers. All these types of structural disorder and the small size of the crystals in clays make it difficult to obtain a good experimental structural data of these minerals by X-ray, neutron or electron diffraction techniques, especially in smectites and illites. The valuable catalytic and adsorptive properties of clays urge us towards having an interest in establishing a firm theoretical understanding of their structure and behaviour.

In dioctahedral phyllosilicates, one of the three symmetrically independent octahedral positions is not occupied by cations; it is a vacant site. The disposition of the hydroxyl groups in the octahedral sheet with respect to this vacancy defines two kind of configurations: *cis*-vacant and *trans*-vacant, when these OH groups are in the same side or in the opposite side with relation to the vacant site, respectively (Fig. 1). The 2:1 layer will have a centre of symmetry in the *trans*-vacant configuration and the *cis*-vacant one will have none (Tsipursky and Drits 1984). In smectites, the octahedral sheet tends to be *cis*-vacant while the illites have mainly a *trans*-vacant disposition (Drits et al. 1998). The *cis*-vacant/*trans*-vacant proportion can be determined in illite/smectites

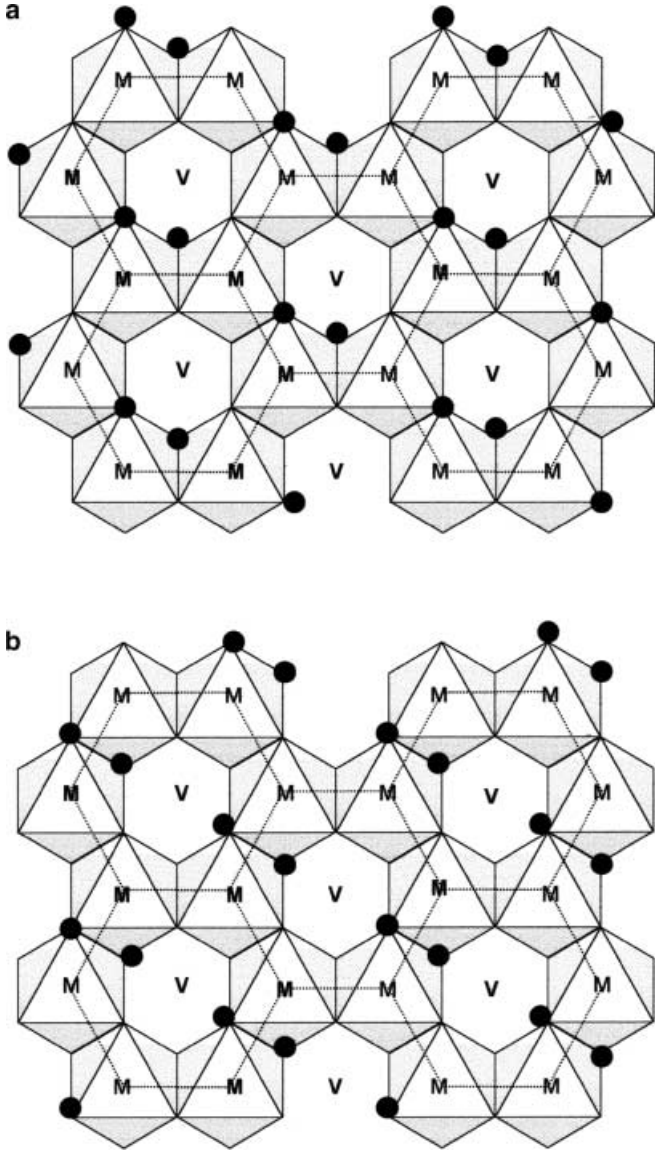

Fig. 1a, b Octahedral sheet of *cis*-vacant (**a**) and *trans*-vacant (**b**) configuration in dioctahedral 2:1 phyllosilicates. *Black circles* represent OH groups, *M* and *V* are the octahedral centres, *V* is the vacant position and *M* is the occupied cation site

(I/S) by X-ray diffraction and thermal analysis, but only with a semiquantitative accuracy (Drits et al. 1998). The *cis*-vacant disposition dehydroxylates at a higher temperature compared to the *trans*-vacant (Cuadros and Altaner 1998). However, it is not clear whether the *trans*-vacant configuration is more stable than the *cis*-vacant. During dehydroxylation, Al^{3+} cations in the *cis*-vacant smectite move from *trans*-octahedral sites to *cis*-octahedral sites, obtaining the *trans*-vacant disposition in the rehydroxylation. This cation arrangement requires additional thermal energy and explains the higher dehydroxylation temperature of the *cis*-vacant smectites (Emmerich et al. 1999). On the other hand, the reactivity of the OH groups depends on the nature of the cations joined to them. Therefore, the cation distribution in the octahedral sheet of these minerals is important in these dehydroxylation processes and other natural transformations. In the bentonite illite/smectite transformations, an increase in Fe segregation was observed with the increase in illite layers (Cuadros et al. 1999). At the same time, the proportion of the *trans*-vacant configurations increases with the proportion of illite; however, no linear relationship between both proportions was obtained in this process (Cuadros and Altaner 1998). One of the aims of this work is to study these *cis*-vacant/*trans*-vacant systems at microscopic scale and the influence of the isomorphous substitution of cations in the octahedral sheet on the crystal lattice geometry of both systems.

Despite the increasing applicability of first-principles quantum-mechanical methods to the solid state, the computational effort of these methods limits their application to large systems with low symmetry, like these systems (Sauer et al. 1994). Atomistic calculations with empirical potentials based on the Born model of the ionic lattice, which employ interatomic potentials to represent the short-range interactions between ions, are fast, and provide enough accuracy for reproducing properties of several framework silicates (Dove 1989; Winkler et al. 1991). These methods have been also applied in layered 2:1 phyllosilicates in a *trans*-vacant disposition with good agreement with experimental structural data (Sainz-Díaz et al. 2001). One of the aims of this work is to extend this study to *cis*-vacant smectites for reproducing the experimental structure of dioctahedral 2:1 phyllosilicates with low interlayer charge and thus to assess the transferability of certain previously published interatomic potentials (Sainz-Díaz et al. 2001) for modelling the structures of these complex minerals.

The H-atom positions are especially difficult to locate in the crystal lattice of clay minerals experimentally by standard X-ray diffraction. Nevertheless, neutron diffraction has given some interesting results with high-quality crystals in micas (Catti et al. 1994). However, this quality of crystal is difficult to obtain in smectites and illites due to the small crystal size and stacking disorder. Therefore, theoretical calculations are very useful to assist in locating the H atoms in the crystal lattice of clay minerals. In this work, we analyse the H-atom positions, O–H bond orientations and H-bonding interactions from our calculations in smectites and illites structures.

Methods

Interatomic potentials are Coulomb interactions between the ionic charges and a short-range function which describes the non-Coulombic interactions between ions, that is the Pauli repulsion at short range and the dispersion forces at longer ranges (Abbot et al. 1989a, b; Collins and Catlow 1992; Winkler et al. 1991). Electrostatic Coulomb interactions are evaluated by the Ewald method using formal charges on all atoms, except for the OH species, whose component atoms have partial charges chosen so as to

reproduce the dipole moment of the OH group. The short-range cation/oxygen interactions are described by Buckingham potentials:

$$E = A\exp(-r/\rho) - Cr^{-6} \quad , \tag{1}$$

where the exponential and the r^{-6} terms describe the repulsive energy and the longer-range attraction, respectively.

In the modelling of all oxygen atoms, except those from hydroxy groups, electronic polarisability effects are taken into account by using the shell model. In this model the atoms are considered to consist of a core comprising the nucleus and tightly bound inner electrons, surrounded by a massless shell of the remaining outer electrons. The core is assigned a charge of $+0.84819e$ and the shell a charge of $-2.84819e$, maintaining the formal value for the overall ionic charge. The shell and core are held together by an ideal harmonic core–shell interaction:

$$E = 1/2\,K_S r^2 \quad , \tag{2}$$

where K_S is the harmonic spring constant and r is the separation between the centres of core and shell.

The O and H atoms within the hydroxyl group are given non-formal charge values, although the overall charge on the hydroxyl molecular ion has a formal charge of $-1e$. The intramolecular OH interaction is described by a Morse potential:

$$E = D\{(1 - \exp[-a(r - r_0)])^2 - 1\} \quad , \tag{3}$$

where r and r_0 are the observed and equilibrium interatomic distances, respectively. Coulomb forces are not included between atoms coupled by a Morse potential, as it is assumed that this potential describes all components of the interactions between both atoms.

Covalent effects are simulated using three-body bond-bending interactions

$$E = 1/2\,k(\theta - \theta_0)^2 \quad , \tag{4}$$

where k is the harmonic three-body force constant, and θ and θ_0 are the observed and ideal bond angles, respectively.

The values of the parameters for the potentials used in this work are described in Table 1. An empirical Al^{3+}–O^{2-} potential has been used for all coordinations (Jackson and Catlow 1988). Although the OH groups are joined to cations of the octahedral sheet, they are close to the cations of the tetrahedral sheet. Then, we include an empirical Si^{4+}_{core}–$O^{1.426-}_{core}$ potential for the Si/OH interactions (Collins and Catlow 1992). Since the isomorphous substitution of Mg and Fe occurs in the octahedral sheet, the Mg–O and Fe–O potentials were also included for both types of oxygens (O^{2-} and OH). The longer-range H bonds (OH…O) are described by an H–O Buckingham potential (Winkler et al. 1991). For modelling the interlayer space interactions with exchange cations, the K–O potential from Post and Burnham (1986), the Na–O and Ca–O potentials from Bush et al. (1994) (Bosenick et al. 2000) and the Mg–O potential from Gale (1997) described quite well the interlayer interactions. All these parameters have been used to model accurately structures and crystal properties of the main rock-forming silicate minerals and layer 2:1 phyllosilicates (Sainz-Díaz et al. 2001). All lattice energy calculations have been performed by means of the GULP code with the Newton-Raphson minimisation method for the lattice relaxation (Gale 1997).

Table 1 Interatomic potential parameters used in this work

	A (eV)	ρ (Å)	C (eV Å^{-6})	Reference
Short-range interactions[a]				
Si^{4+}–O^{2-}	1283.9073	0.3205	10.6616	[b]
Si^{4+}–$O^{1.426-}$	999.98	0.3012	0.0	[b]
Al^{3+}–$O^{1.426-}$	1142.6775	0.2991	0.0	[c]
Al^{3+}–O^{2-}	1460.3	0.2991	0.0	[b]
Fe^{3+}–O^{2-d}	3219.335	0.2641	0.0	[e]
Mg^{2+}–$O^{1.426-}$	1142.6775	0.2945	0.0	[b]
Mg^{2+}–O^{2-}	1428.5	0.2945	0.0	[b]
K^{+}–O^{2-}	65269.71	0.2130	0.0	[b]
Na^{+}–O^{2-}	1271.504	0.3000	0.0	[e]
Mg^{2+}(interlayer)–O^{2-}	946.627	0.31813	0.0	[f]
Ca^{2+}–O^{2-}	2272.74	0.2986	0.0	[e]
O^{2-}–O^{2-}	22764.0	0.149	27.88	[b]
$H^{0.426+}$–O^{2-}	325.0	0.25	0.0	[b]
Short-range interactions[g]	D (eV)	a (Å^{-1})	r_0 (Å)	
$H^{0.426+}$–$O^{1.426-}$	7.0525	2.1986	0.9485	[b]
Shell–core interaction	K (eV Å^{-2})			
$O^{0.86902-}_{core}$–$O^{2.86902-}_{shell}$	74.92			[b]
Three-body bond-bending[h]	k (eV rad^{-2})	θ_0 (°)		
O^{2-}–Si^{4+}–O^{2-}	2.09724	109.47		[b]
O^{2-}–Al^{3+}(T)–O^{2-}	2.09724	109.47		[b]
O^{2-}–M(Oc)–O^{2-}	2.09724	90		[b]
O^{2-}–M(Oc)–$O^{1.426-}$	2.09724	90		
$O^{1.426-}$–M(Oc)–$O^{1.426-}$	2.09724	90		

[a] Parameters for the Buckingham potentials between cation cores and oxygen shells. When the parameter $C = 0.0$, the function takes the form of Born-Mayer potentials. Cutoff at 12 Å
[b] Winkler et al. (1991)
[c] Schröder et al. (1992)
[d] O^{2-}_{shell} or $O^{1.426-}_{core}$
[e] Bush et al. (1994)
[f] Gale (1997)
[g] Modified Morse potential between cores
[h] T in the tetrahedral sheet; Oc in the octahedral coordination; M any cation in the octahedral sheet, Al^{3+}, Fe^{3+} and Mg^{2+}

Partial occupancies of Si and Al were included in the crystallographic positions of the tetrahedral sheet, since disordered tetrahedral cation distributions were found experimentally in micas (Herrero and Sanz 1991). In illite/smectite systems, spectroscopic studies and inverse MC simulations showed an MgMg pair avoidance and a partial short-range Fe segregation in the octahedral sheet, but no specific ordering was found (Cuadros et al. 1999). Besides, the cation ordering in the octahedral sheet does not significantly affect the crystal lattice parameters of these systems, since the experimental data are averaged values. Therefore, partial occupancies of Al, Mg and Fe have been also included, taking into account the chemical composition of these cations. This approach treats each distinct cation site as equivalent in each unit cell, and is a type of mean-field approach, often called the virtual crystal approximation. This approximation has been used to great effect in a number of studies on the behaviour of disordered crystals from a structural perspective (Winkler et al. 1991; Dove et al. 1993; Dove and Redfern 1997). Hence, this approximation can be considered valid by the good agreement obtained with the experimental data in theoretical studies on 2:1 phyllosilicates with *trans*-vacant configuration (Sainz-Díaz et al. 2001).

In the illite/smectite samples, no experimental atomic coordinates were available. Nevertheless, the initial geometries were taken from the models proposed by Tsipursky and Drits (1984) by means of oblique-texture electron diffraction studies of dioctahedral smectites. The initial hydrogen positions of smectites and illites were taken from the Giese (1979) studies on pyrophyllite, and optimised previously by us.

Results

A wide range of compositions generating different tetrahedral, octahedral and interlayer charges for I/S mineralogical species is considered (Table 2) by including different cation substitutions of Al^{3+} by Mg^{2+} and Fe^{3+}, and Si^{4+} by Al^{3+} in the octahedral and tetrahedral sheet, respectively. Some of the samples modelled in this work have no tetrahedral charge (samples 1–3), or a high tetrahedral charge (14–17). There are also a sample without octahedral charge (5), a sample with a very high octahedral charge (6), another with a very low interlayer charge (4) and samples with a high interlayer charge (6, 15, and 17). Different interlayer cations have been used (K^+, Na^+, Mg^{2+}, and Ca^{2+}). Finally, samples with a very high Fe^{3+} content in the octahedral sheet have also been included (15 and 16).

Table 2 Chemical composition of the phyllosilicate samples studied. Structural formulae on the unit-cell basis for $O_{20}(OH)_4$

Sample	Si^{4+} (T)	Al^{3+} (T)	Al^{3+} (Oc)	Mg^{2+} (Oc)	Fe^{3+} (Oc)	Interlayer cation
1	8		3.5	0.5		$Na_{0.5}$
2	8		3	1		Na_1
3	8		2.8	0.7	0.5	$K_{0.7}$
4	7.9	0.1	3.9	0.1		$K_{0.2}$
5	7.6	0.4	4			$Na_{0.4}$
6	7.6	0.4	2.4	1.6		K_2
7	7.2	0.8	3.7	0.3		$K_{1.1}$
8	7.2	0.8	3.5	0.5		$K_{1.3}$
9	7.2	0.8	3.3	0.7		$Na_{1.5}$
10	7.2	0.8	3.3	0.7		$Mg_{0.75}$
11	7.2	0.8	3.3	0.7		$Ca_{0.75}$
12	7.2	0.8	3	0.5	0.5	$Na_{1.3}$
13	7.2	0.8	3	0.5	0.5	$K_{1.3}$
14	7.13	0.87	3.3	0.7		$K_{1.57}$
15	7.13	0.87	2	1	1	$K_{1.87}$
16	7	1	1.8	0.4	1.8	$K_{1.4}$
17	6.5	1.5	3.5	0.5		K_2

The unit-cell parameters of the *cis*-vacant calculated structures are described in Table 3 including also the values corresponding to the *trans*-vacant configuration (Sainz-Díaz et al. 2001) and the experimental values. In general, the calculated values of the cell parameters a, c and β are lower in the *cis*-vacant configurations than in the *trans*-vacant structures. A similar phenomenon was found experimentally by Drits and McCarty (1996) in the parameters c and β on illites and illite/smectite systems. The parameter b is slightly higher in the *cis*-vacant structures than in the *trans*-vacant.

We can calculate the crystal lattice parameters, taking into account the *cis*/*trans* proportion for each composition. These values will be a statistically weighted sum of the values for each configuration (*cis* or *trans*). With these weighted calculations the agreement between experimental and calculated values is higher than if considering only the *cis*- or the *trans*-vacant values (Table 3). This means that the *cis*/*trans* proportion is important to determine the lattice parameters, since they are average values of both types of configurations. However, this agreement is not so good in cases where the *cis*-vacant configuration was considered negligible in the experimental studies. This fact was expected, since these experimental *cis*/*trans* proportions were only approximate and semiquantitative values. Tsipurski and Drits (1984) classified their samples in three groups, taking into account the value of the modulus of the projection of the c axis on the (a, b) plane ($|c.\cos\beta|$). This factor could be considerably greater than $a/3$ (0% of *cis*-vacant), smaller than $a/3$ (75–100% of *cis*-vacant) or equal or slightly higher than $a/3$ (intermediate proportion of *cis*-vacant). Hence, the parameter ($\tau = |c.\cos\beta|/a$) can be one way to determine the proportion of *cis*-vacant or *trans*-vacant layers. This parameter τ can be calculated from the d values of the XRD reflection lines and it will be a statistically weighted sum of the values for each configuration *cis* or *trans* (considering a random interstratification of *cis* and *trans*-vacant layers). Experimental studies need to find the values of τ for pure *cis*-vacant or *trans*-vacant configurations for the fitting procedure in the XRD patterns and the quantitative determination of *cis*/*trans* proportion. However, different values have been reported for similar samples [$\tau_{cis} = 0.308$ and $\tau_{trans} = 0.383$ (Drits et al. 1993; McCarty and Reynolds 1995); $\tau_{cis} = 0.302$ and $\tau_{trans} = 0.400$ (Drits and McCarty 1996)]. Our calculations permit us to determine these values for pure *cis*-vacant and pure *trans*-vacant layers for cation compositions (samples 8, 13–15 and 17) similar to experimental samples [$K_{(x+y)}(Si_{8-x}Al_x)(Al_{4-y}Mg_yFe^{3+}_z)O_{20}(OH)_4$, where x, y and z are in the ranges of 0.8–1.5, 0.5–1 and 0–1, respectively; McCarty and Reynolds 1995]. Then, the average values of τ for 8, 13–15 and 17 for the *cis*-vacant and *trans*-vacant structures are 0.303

Table 3 Structural features of the smectites/illites studied in *cis*-vacant and *trans*-vacant configurations

Sample	*a* (Å)			*b* (Å)			*c* (Å)			*β* (degrees)[a]			ΔE[b]	*cis*[c]
	cis	*trans*	Exp.[d]	*cis*	*trans*	Exp.[d]	*cis*	*trans*	Exp.[d]	*cis*	*trans*	Exp.[d]		
1	5.16	5.22	5.18 (5.17)	9.02	8.89	8.98 (8.99)	10.04	10.20	10.10 (10.07)	99.8	101.3	99.5 (99.9)	−1.45	0.64
2	5.16	5.23	5.18 (5.19)	9.03	8.90	8.97 (8.97)	10.03	10.20	10.05 (10.09)	99.1	105.7	100.4 (101.7)	3.09	0.22
3	5.14	5.23	5.18 (5.20)	9.02	8.84	8.97 (8.89)	10.07	10.26	10.20 (10.20)	99.0	103.3	101.3 (102.0)	−9.36	0.98
4	5.16	5.20	5.18 (5.17)	9.02	8.90	8.98 (9.00)	10.35	10.60	10.10 (10.36)	99.6	102.2	99.5 (99.9)	−3.20	0.78
5	5.15	5.21	5.18 (5.16)	9.01	8.89	8.98 (8.99)	10.00	10.12	10.10 (10.02)	100.1	100.8	99.6 (100.2)	−5.79	0.91
6	5.17	5.20	5.18 (5.18)	9.02	8.92	8.97 (8.99)	9.90	9.96	10.07 (9.92)	98.9	102.0	99.6 (99.5)	11.19	0.01
7	5.17	5.20	5.18 (5.19)	9.03	8.90	8.98 (8.94)	10.03	10.19	10.05 (10.14)	99.3	102.4	101.4 (101.5)	−4.82	0.87
8	5.17	5.22	5.18 (5.20)	9.03	8.91	8.98 (8.95)	9.99	10.15	10.05 (10.10)	99.2	102.5	101.4 (101.4)	−2.89	0.76
9	5.17	5.23	5.18 (5.21)	9.03	8.92	8.98 (8.95)	9.97	10.10	10.05 (10.06)	100.4	105.0	101.4 (103.6)	1.16	0.39
10	5.16	5.24	5.18 (5.19)	9.02	8.89	8.97 (8.97)	9.78	9.48	10.10 (9.70)	99.5	96.7	100.5 (98.7)	6.08	0.08
11	5.17	5.23	5.18 (5.21)	9.02	8.91	8.98 (8.94)	9.85	9.75	10.05 (9.78)	99.4	98.4	101.4 (98.7)	0.58	0.44
12	5.15	5.22	5.18 (5.18)	9.01	8.85	8.97 (8.94)	9.98	10.04	10.10 (10.01)	99.3	100.4	100.5 (99.8)	−11.50	0.99
13	5.15	5.23	5.18 (5.18)	9.02	8.86	8.97 (8.95)	10.03	10.16	10.10 (10.09)	99.0	102.3	100.5 (100.4)	−11.35	0.99
14	5.18	5.22	5.18 (5.21)	9.04	8.93	8.98 (8.96)	9.95	10.08	10.05 (10.04)	99.1	102.5	101.4 (101.5)	0.21	0.48
15	5.13	5.22	5.18 (5.17)	9.00	8.81	8.97 (8.92)	10.03	10.09	10.10 (10.06)	98.7	102.0	100.5 (100.2)	−13.64	0.99
16	5.11	5.23	5.18 (5.19)	8.98	8.57	9.01 (8.69)	9.77	10.29	10.20 (10.14)	100.7	101.4	101.3 (101.2)	9.65	0.02
17	5.18	5.22		9.04	8.94		9.90	10.03		99.1	102.3		−1.54	0.65

[a] In all cases, $\alpha = \gamma = 90°$

[b] $\Delta E = E_{cis} - E_{trans}$ in kJ mol^{-1} unit cell

[c] Proportion of *cis*-vacant layers from the calculated ΔE

[d] From samples with composition similar to our samples. *Values in brackets* represent theoretical results taking into account the experimental *cis*/*trans* ratio (Tsipurski and Drits 1998) corrected by our calculated τ values

and 0.412, respectively. These values are close to the experimental one from Drits and McCarty (1996) and can be very useful for further XRD refinement studies. Thus, we can determine the *cis*-vacant proportion (P_{cis}) of the experimental samples of Tsipursky and Drits (1984) by means of the equation:

$$P_{cis} = 100\,x(\tau_{trans} - \tau)/(\tau_{trans} - \tau_{cis}) \ , \quad (5)$$

where τ_{trans} (0.412) and τ_{cis} (0.303) are our calculated values and τ is the experimental value of the sample. This corrected proportion *cis*/*trans* was applied to our calculated lattice parameters, following Eq. (6) as explained above:

$$h = h_{cis}P_{cis} + h_{trans}(1 - P_{cis}) \ , \quad (6)$$

where h represents the calculated values of a, b, c, and β parameters in each case for each configuration and h_{cis} and h_{trans} are the calculated values for the *cis*- and *trans*-vacant configurations, respectively. A better agreement with the experimental values was obtained with this approximation (Table 3).

Cation substitution effect on the lattice parameters

While in the *trans*-vacant samples with Ca^{2+} or Mg^{2+} as interlayer cations (10 and 11) the calculated values of c and β are lower than in the rest of the series, these differences are not so significant in the *cis*-vacant configurations. Probably these divalent cations fit better in a *cis*-vacant system than in a *trans*-vacant one. On the other hand, the high theoretical value of c with respect to the experiment found in the *trans*-vacant sample with very low interlayer charge (4) is lower and closer to the experiment in the *cis*-vacant configurations. Probably this configuration is more stable for this composition.

As in the *trans*-vacant samples, a slight increase of b is observed in the *cis*-vacant with the increase of the interlayer charge but only in the order of 0.1%. The increase in Fe content produces a decrease in a and b, presenting linear relationships in both parameters. Thus, in potassium samples with a composition of $K_{(x+y)}(Si_{8-x}Al_x)(Al_{4-y}Mg_yFe_z)O_{20}(OH)_4$ (where $x = 0.8$–1 and $y = 0.4$–1) the Fe substitution effect on a and b can be expressed quantitatively by the equations:

$$a = 5.174 - 0.038(Fe^{3+}) \ (R^2 = 0.9565) \quad (7)$$

$$b = 9.038 - 0.033(Fe^{3+}) \ (R^2 = 0.9847) \ , \quad (8)$$

where Fe^{3+} represents the Fe content for unit cell. In the *trans*-vacant samples the Fe effect on a was negligible and the Fe effect on b was higher than in the *cis*-vacant. On the other hand, in the *cis*-vacant structure a decrease of parameter c is observed with the increase of the Mg content, presenting a linear correlation. Thus, in potassium samples with a unit-cell composition $K_{(0.8+x)}(Si_{7.2}Al_{0.8})(Al_{4-x}Mg_x)O_{20}(OH)_4$, the Mg substitution effect on c (in Å) can be expressed quantitatively by the equation:

$$c = 10.045 - 0.093\,Mg \ (R^2 = 0.9605) \ , \quad (9)$$

where Mg represents the Mg content for $O_{20}(OH)_4$ unit cell. This effect is lower than in *trans*-vacant configurations (slope = −0.18, Sainz-Díaz et al. 2001). The increase in Mg content in the octahedral sheet produces an increase in the interlayer charge and attractive interactions in the interlayer space, decreasing the interlayer d(001) spacing. A similar relationship is found in experimental results of illite/smectites with a high proportion of *cis*-vacant layers (Tsipursky and Drits 1984), close to our results with the equation:

$$c = 10.18 - 0.12\,Mg \ (R = 0.7450) \ . \quad (10)$$

The intercept is slightly higher than in Eq. (9), due to the contribution of the small proportion of *trans*-vacant layers in the experimental samples. The low value of R in Eq. (10) is due to the high dispersion of compositions in the natural samples.

Cation substitution effect on the *cis*- and *trans*-vacant proportion

Small energy differences are found between the *cis*-vacant and *trans*-vacant configurations for each composition (Table 3). In general, from our calculations the higher the smectitic composition the lower the energy of the *cis*-vacant configuration (lower values of ΔE in Table 3). This fact is consistent with the experimental behaviour in I/S minerals, where the *cis*-vacant proportion is higher when the smectite content is also higher (Drits et al. 1998). In samples with a very high Mg^{2+} content in the octahedral sheet (6), the calculated *trans*-vacant configuration is more stable than *cis*-vacant, in accord with experimental results (McCarty and Reynolds 1995). Analogously, in calculations of samples with a very high Fe^{3+} content (16), the *trans*-vacant configuration is also more stable than the *cis*-vacant, as observed experimentally in nontronites (Manceau et al. 2000). An increase of the calculated relative energy ($\Delta E = E_{cis} - E_{trans}$) with the increase in Mg content is observed with a linear relationship (Fig. 2, $R^2 = 0.9711$). In the same way, an increase of calculated ΔE with the increase in interlayer charge was observed with a linear relationship (Fig. 2, $R^2 = 0.9877$). A similar behaviour is

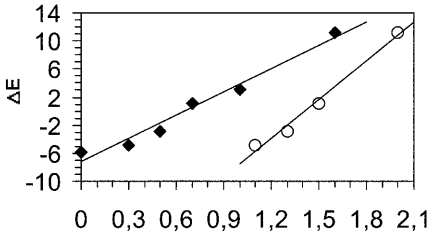

Fig. 2 Effect of the Mg content (per unit cell, *closed symbols*) and interlayer charge (per unit cell, *open symbols*) on the energy difference (ΔE) between *cis*- and *trans*-vacant configurations (in kJ mol^{-1} unit $cell^{-1}$)

observed experimentally; the illitic samples and micas (higher interlayer charge) have mainly a *trans*-vacant configuration, whereas in the smectitic samples (lower interlayer charge) the proportion of *cis*-vacant configuration is higher.

Recent experimental results on the distribution of octahedral cations in illites and illite-smectites (McCarty and Reynolds 1995; Drits and McCarty 1996) found the absence of coexisting *cis*- and *trans*-vacant configurations within the same octahedral sheet, where both configurations belong to different layers. Then, the *cis*/*trans* population for each sample at a given temperature may be calculated by means of a standard population analysis method. Thus, taking into account the relative energy of *cis* with respect to the *trans* configuration, the proportion of *cis*-vacant configuration at 300 K and normal pressure and as ideal models was calculated (Table 3). In the relationship between *cis*/*trans* ratio and composition, we have found trends theoretically similar to the experimental results. However, the energy differences between both configurations are small and many external factors can affect this *cis*/*trans* proportion in nature and in the *cis*/*trans* transformation. This means that no predictive correlation can be obtained experimentally and theoretically about the direct effect of cation substitution on the *cis*/*trans* proportion. Experimental studies found that smectites from the same deposit with very close chemical composition may have different *cis*-/*trans*-vacant layer proportion, finding also the same observation on illites (Tsipursky and Drits 1984; Drits et al. 1993). Their interpretation is that different physical conditions during the illitisation were responsible for the structural variations for both mechanisms dissolution/precipitation and solid-phase transformation. In general, the amount of *cis*-vacant layers decreases with the increase in illite layer proportion in natural I/S samples (Drits et al. 1996; Cuadros and Altaner 1998), but no direct correlation has been found. This *cis*/*trans* transformation during the illitisation is faster in a dissolution-reprecipitation process, whereas in a solid-phase illitisation the *cis*/*trans* change is much slower or it does not occur. Probably the *cis*/*trans* relative energy has a more significant role in a solid-phase illitization that in the another mechanism where different kinetics or external factors can participate.

On the other hand, the formation of only *trans*-vacant configurations in the rehydroxylation of dehydroxylated smectites does not mean that the *trans*-vacant is the most stable configuration. From our calculations, only some samples have the *trans*-vacant as the most stable, with a small energy difference. Probably the path reaction between the dehydroxylated structure with pentacoordinate Al atoms (Drits et al. 1998; Emmerich et al. 1999) to the *trans*-vacant rehydroxylated structure has intermediates or transition states with lower energy than necessary to obtain the *cis*-vacant one.

Hydroxy groups in *cis*-vacant and *trans*-vacant configurations

The calculated values of OH-bond length, the orientation angle (ρ) of the O–H bond with respect to the (001) plane (Giese 1979), and the main distances to the surrounding tetrahedral oxygens are presented in Table 4. Both *cis*-vacant and *trans*-vacant configurations have been included for comparative studies. H1, H2, and H3 represent the distances of the H atoms to the basal tet-

Table 4 Structural features of the hydroxy groups in the *cis*-vacant (*cis*) and *trans*-vacant (*trans*) configurations of illite/smectites (distances in Å, angles in degrees)

Sample	d(OH)[a]		ρ(OH)[b]		H1[c]		H2[c]		H3[c]		H4/H5[c]	
	cis	*trans*	*cis*	*trans*	*cis*	*trans*	*cis*	*trans*	*cis*	*trans*	*cis*	*trans*
1	0.979	0.979	51.2	50.8	2.54	2.57	3.13	3.17	3.19	3.17	2.84	2.85
2	0.976	0.977	37.2	31.3	2.53	2.55	2.97	2.88	2.92	2.88	2.83	2.82
3	0.981	0.980	37.5	37.7	2.57	2.53	2.93	2.95	2.93	2.95	2.79	2.78
4	0.981	0.981	55.7	55.8	2.55	2.54	3.21	3.26	3.21	3.26	2.87	2.85
5	0.981	0.981	54.2	54.3	2.51	2.53	3.26	3.23	3.20	3.23	2.84	2.84
6	0.979	0.982	9.4	2.8	2.71	2.78	2.60	2.55	2.63	2.55	2.87	2.88
7	0.978	0.979	44.5	40.8	2.48	2.48	3.10	3.03	3.10	3.03	2.82	2.81
8	0.977	0.979	38.7	33.2	2.48	2.50	3.03	2.92	2.97	2.92	2.81	2.81
9	0.977	0.979	31.0	23.3	2.48	2.54	2.87	2.80	2.93	2.80	2.81	
10	0.977	0.979	31.6	19.5	2.44	2.58	2.89	2.75	2.83	2.75		
11	0.979	0.979	31.6	21.9	2.46	2.55	2.92	2.77	2.87	2.77		2.80
12	0.982	0.982	32.1	27.4	2.51	2.50	2.90	2.82	2.87	2.82	2.77	2.76
13	0.982	0.982	31.6	28.0	2.54	2.52	2.87	2.84	2.90	2.84	2.77	2.76
14	0.977	0.977	30.0	21.2	2.50	2.57	2.85	2.77	2.91	2.77		
15	0.987	0.988	17.0	12.1	2.73	2.71	2.69	2.65	2.71	2.65		
16		0.999	52.9	26.3	2.57	2.52	3.02	2.80	3.02	2.80	2.85	2.62
17	0.978	0.980	27.6	19.4	2.46	2.55	2.91	2.76	2.84	2.76	2.78	2.80

[a] O–H bond length
[b] Orientation angle of OH bond with respect to (001) plane
[c] See Fig. 3

rahedral oxygens. H1 is the distance between the H atom with the basal oxygen that is closer to the plane formed by the H atom and the dioctahedral sharing edge of the OH group (the basal tetrahedral oxygen will have the same fractional coordinate y with respect to the b axis as the H atom). H2 and H3 are the distances of the H atom to the basal oxygens that are vicinal to the former one of H1 (Fig. 3). H4 and H5 represent the distances between this H atom and the apical oxygens of the tetrahedra that are in front of it (Fig. 3). In general, the H-atom geometry is controlled by the interactions with these oxygens and the interlayer cation.

The O–H bond lengths of *cis*-vacant and *trans*-vacant are very similar and no significant difference is detected. For both configurations, an increase in O–H bond length with the increase in Fe^{3+} content is observed (samples 3, 12, 13 and 15). Obviously, the increase in O–H bond length is related to a decrease in ν(OH) vibration frequency. This is consistent with the experimental values of the stretching vibrational frequency ν(OH) of the M–OH–M groups, which decrease with the increase in Fe content (Besson and Drits 1997). This fact has been corroborated by means of quantum-mechanical calculations of molecular clusters representative of these M–OH–M′ systems (Sainz-Díaz et al. 2000).

In general, the orientation angle (ρ) is higher in the *cis*-vacant system than in the *trans*-vacant (Table 4). In the samples 1, 3–5, where the interlayer charge is low, the ρ values are similar for both configurations. A good linear relationship between the ρ values of the *cis*-vacant and *trans*-vacant configurations is observed (Fig. 4a), showing a similar behaviour of the OH groups for both configurations.

Since the hydroxy group orientation depends largely on the cation charges, we can correlate the angle ρ with the tetrahedral, octahedral and interlayer charges. Taking into account that partial occupancies of cations are used in the tetrahedral, octahedral and interlayer cation sites, a random distribution of these cations has been considered in these layers. Hence, the values of ρ will be averaged values, as in most experimental data. For both *cis*-vacant and *trans*-vacant (Fig. 4b) configurations, ρ decreases with the increase in interlayer charge with a linear relationship for the most of our series, following the expressions:

$$\rho = 61.83 - 22.22\,Q_{IC} \quad (R^2 = 0.8732,\ \text{for } cis\text{-vacant}) \tag{11}$$

$$\rho = 61.83 - 25.80\,Q_{IC} \quad (R^2 = 0.9095,\ \text{for } trans\text{-vacant})\ , \tag{12}$$

where Q_{IC} is the interlayer charge for unit cell. This is consistent with previous electrostatic energy calculations on dioctahedral micas (Giese 1979). From Eqs. (11) and (12), we can conclude that the interlayer charge effect on ρ is similar for both kinds of configurations, although this effect is slightly higher in the *trans*-vacant.

We have performed multiple regressions correlating the ρ values with the Mg and tetrahedral Al contents, in order to observe the effect of the tetrahedral and octahedral charges on the OH orientation angle (ρ). Thus, the following expressions were obtained:

$$\rho = 61.49 - 1.14\,T(\pm 0.15) - 1.13\,M(\pm 0.09) \quad (R^2 = 0.9452,\ \text{for } cis\text{-vacant}) \tag{13}$$

$$\rho = 62.76 - 1.64\,T(\pm 0.13) - 1.31\,M(\pm 0.08) \quad (R^2 = 0.9677,\ \text{for } trans\text{-vacant})\ , \tag{14}$$

where T and M represent the percentage (%) of Al in tetrahedral sheet and Mg in octahedral sheet, respec-

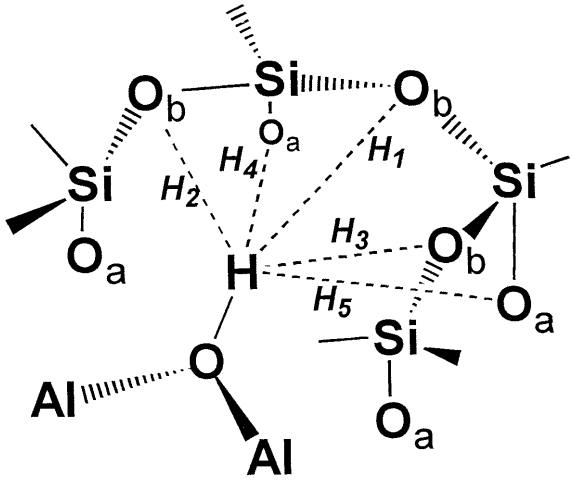

Fig. 3 Definition of the main distances of the H atoms of OH groups to the surrounding oxygens of the tetrahedral sheet. O_a and O_b represent the apical and basal tetrahedral oxygens, respectively

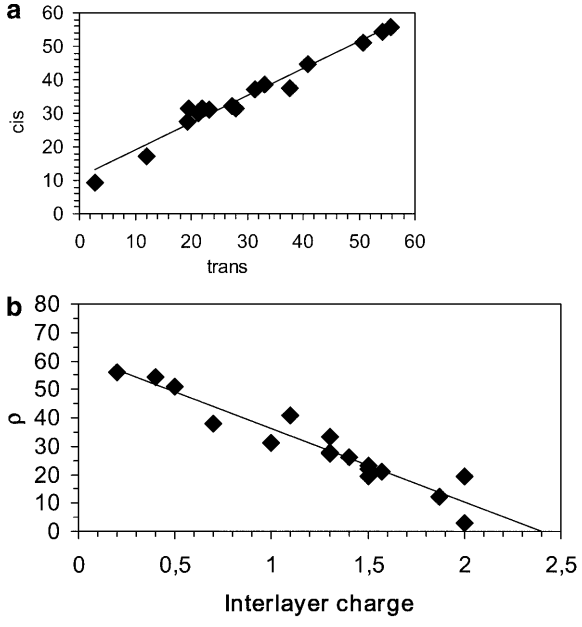

Fig. 4a, b Orientation angle (in degrees) of the hydroxy groups (ρ). Relationship between the ρ values in *cis*- and *trans*-vacant configurations (**a**), and effect of the interlayer charge (per unit cell) on ρ for *trans*-vacant structures (**b**)

tively. This analysis can be considered as successful in that ρ can be predicted with reasonable accuracy for our samples. Hence, the effect of the tetrahedral charge is higher than that of the octahedral charge in the *trans*-vacant configurations, while both effects are similar in the *cis*-vacant systems. In both configurations, the increase of the tetrahedral or octahedral charge produces a decrease of ρ.

The H_n ($n = 1$, 2, 3, 4 and 5) distances depend significantly on ρ and O–H bond length. The lower ρ, the higher H1, and the lower H2 and H3. These H_n values for *cis*- and *trans*-vacant configurations are similar to each other, and the small differences follow the same trend of ρ. The differences between H2 and H3 are not significant, and H4 and H5 have values similar to each other. This means a high symmetry of the O–H bond orientation with respect to the tetrahedra neighbourhood. H1 is the shortest O...H distance (2.4–2.7 Å), and H4 and H5 are higher (2.6–3.3 Å, and 2.8–2.9 Å for H2/H3 and H4/H5, respectively). H1 decreases with the increase of the tetrahedral charge (Fig. 5). The substitution of Al in the tetrahedra produces a charge increase in the tetrahedral oxygens that increases the H-bonding interactions with the H atom, producing a decrease of H1. This is consistent with spectroscopic studies of stretching vibrations of OH groups [ν(OH)], where this effect produces a frequency decrease (Besson and Drits 1997). A decrease in H2 is observed with the increase of interlayer charge (Fig. 5). The interlayer charge increase yields an increase in the interlayer cation concentration. The repulsion between these cations and the H atom produces a decrease of ρ and hence a decrease of H2. These theoretical values are consistent with experimental O...H distances from powder neutron diffraction on muscovite ($K_{1.8}Na_{0.14}$ ($Al_{3.26}Fe_{0.46}Mg_{0.32}Ti_{0.06}$) ($Si_{6.4}Al_{1.6}$)$O_{20}(OH)_4$) (Catti et al. 1994), where H1 = 2.64 Å and H2/H3 = 2.62–2.67 Å. Taking into account the composition of this muscovite (tetrahedral charge = 1.6, interlayer charge = 1.94) and Fig. 5, our calculated values would be 2.5 and 2.64 Å for H1 and H2, respectively.

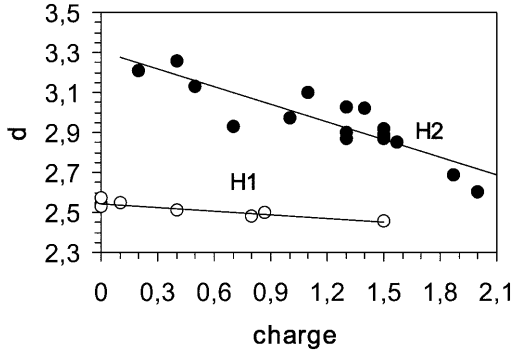

Fig. 5 Effect of the tetrahedral charge on the H1 (H...O) distance (*open circles*), and the interlayer charge on H2 (*solid circles*). Distances (*d*) are in Å and charges are per unit cell

Conclusions

The use of a suitable transferable empirical potential set can reproduce theoretically the main structural properties of dioctahedral 2:1 phyllosilicates with a wide range of interlayer charge. Both kinds of configurations, *cis*- and *trans*-vacant, are well reproduced by means of these calculations. Apart from quantitative *cis*-/*trans*-vacant determination, accurate values of τ for pure *cis*-vacant and *trans*-vacant configurations are difficult to obtain experimentally. These τ values can be predicted by means of our calculations, allowing more accurate calculation of the *cis*-/*trans*-vacant ratio. Therefore, taking into account the experimental *cis*-/*trans*-vacant proportion, the calculated structures are in agreement with experiment for the main structural features of the crystal lattice.

Octahedral and tetrahedral cation substitution effects on the main crystal lattice parameters of *cis*-vacant systems are lower than in the *trans*-vacant configurations, showing good linear correlations. Our theoretical results are consistent with the experiment in the cases where this cation substitution effect has been detected experimentally. The good assessment of this force field encouraged us to use it in an order/disorder study of the cation distribution in these minerals, which is in progress and will appear in forthcoming papers.

The energy differences between the *cis*-vacant and *trans*-vacant configurations are small for a certain composition. Nevertheless, we found good agreement with experiments. In our calculations a higher population of *cis*-vacant layers is found in the more smectitic samples, whereas the *trans*-vacant population is higher in the illitic samples, as found experimentally. In the cation substitution effect on the *cis*-/*trans*-vacant relative population similar trends were found theoretically and experimentally, especially in the effects of Mg and Fe content. However, no predictive correlation can be obtained with both theoretical and experimental approaches. This fact can be explained by the small energy difference between both configurations, and any external factor can alter this *cis*/*trans* ratio and the *cis*/*trans* transformation mechanism in nature.

The calculated OH-bond length is slightly higher than the experimental values, and no significant difference was found between *cis*- and *trans*-vacant configurations. Nevertheless, an increase in O–H bond length with Fe content is found, in accord with the experimental fact of the decrease of ν(OH) with increase in Fe content. The orientation angle of the O–H bond with respect to the (001) plane (ρ) is slightly higher in the *cis*-vacant system than in the *trans*-vacant. Nevertheless, a similar behaviour of ρ with the cation substitution was found for both kinds of configurations. A decrease of ρ was observed with the increase of interlayer charge. The increase of interlayer charge produces an increase of interlayer cation population. The higher repulsion interaction between the H atom and interlayer cation

makes ρ lower. This interaction produces the same effect on the H2 (H...O) distance. The higher interlayer charge, the shorter the H2 distance is. The H1 (H...O) distance decreases with the increase of the tetrahedral charge. Our calculations reproduce the increase in the H-bonding interactions with the tetrahedral Al substitution, detected experimentally in the ν(OH) frequencies. These H_n (H...O) distance variations are similar for both *cis*- and *trans*-vacant configurations. Therefore, our calculations can predict the OH group geometry in these minerals that is not possible to determine experimentally, and this theoretical study can be a useful tool for experimental work.

Acknowledgements The authors are grateful to J. Gale for his fruitful help and for permitting us to use the GULP programme, and for the financial support of Acciones Integradas UK/Spain joint research programme, (HB1998-0193) NERC (M.T. Dove), Royal Society of UK and MEC of Spain (C.I. Sainz-Díaz), and the PB97–1205 DGES project (A. Hernández-Laguna).

References

Abbot RN Jr, Post JE, Burnham CW (1989a) Treatment of the hydroxyl in structure-energy calculations. Am Mineral 74: 141–150

Abbot RN Jr, Burnham CW, Post JE (1989b) Hydrogen in humite-group minerals: structure-energy calculations. Am Mineral 74: 1300–1306

Besson G, Drits VA (1997) Refined relationship between chemical composition of dioctahedral fine-grained micaceous minerals and their infrared spectra within the OH stretching region. Clays Clay Miner 45: 170–183

Bosenick A, Dove MT, Geiger CA (2000) Simulation studies of pyrope-grossular solid solutions. Phys Chem Miner 27: 398–418

Bush TS, Gale JD, Catlow CRA, Battle PD (1994) Self-consistent interatomic potentials for the simulation of binary and ternary oxides. J Mat Chem 4: 831–837

Catti M, Ferraris G, Hull S, Pavese A (1994) Powder neutron diffraction study of 2M1 muscovite at room pressure and at 2 Gpa. Eur J Mineral 6: 171–178

Collins DR, Catlow CRA (1992) Computer simulations of structures and cohesive properties of micas. Am Mineral 77: 1172–1181

Cuadros J, Altaner SP (1998) Compositional and structural features of the octahedral sheet in mixed-layer illite/smectite from bentonites. Eur J Mineral 10: 111–124

Cuadros J, Sainz-Díaz C, Ramirez R, Hernández-Laguna A (1999) Analysis of Fe segregation in the octahedral sheet of bentonitic illite-smectite by means of FT-IR, ^{27}Al MAS NMR and reverse Monte Carlo simulations. Am J Sci 299: 289–308

Dove MT (1989) On the computer modeling of diopside: toward a transferable potential for silicate minerals. Am Mineral 74: 774–779

Dove MT, Redfern SAT (1997) Lattice simulation studies of the ferroelastic phase transitions in $(Na,K)AlSi_3O_8$ and $(Sr,Ca)Al_2Si_2O_8$ feldspar solid solutions. Am Mineral 82: 8–15

Dove MT, Cool T, Palmer DC, Putnis A, Salje EKH, Winkler B (1993) On the role of Al/Si ordering in the cubic–tetragonal phase transition in leucite. Am Mineral 78: 486–492

Drits VA, McCarty DK (1996) The nature of diffraction effects from illite and illite-smectite consisting of interstratified *trans*-vacant and *cis*-vacant 2:1 layers: a semiquantitative technique for determination of layer-type content. Am Mineral 81: 852–863

Drits VA, Weber F, Salyn AL, Tsipursky SI (1993) X-ray identification of one-layer illite varieties: application to the study of illites around uranium deposits of Canada. Clays Clay Miner 41: 389–398

Drits VA, Salyn AL, Sucha V (1996) Structural transformation of interstratified illite-smectites from Dolná ves hydrothermal deposits: dynamics and mechanisms. Clays Clay Miner 44: 181–190

Drits VA, Lindgreen H, Salyn AL, Ylagan R, McCarty DK (1998) Semiquantitative determination of *trans*-vacant and *cis*-vacant 2:1 layers in illites and illite-smectites by thermal analysis and X-ray diffraction. Am Mineral 83: 1188–1198

Emmerich K, Madsen FT, Kahr G (1999) Dehydroxylation behavior of heat-treated and steam-treated homoionic *cis*-vacant montmorillonites. Clays Clay Miner 47: 591–604

Gale JD (1997) GULP – a computer program for the symmetry adapted simulation of solids. J Chem Soc Faraday Trans 93: 629

Giese RF Jr (1979) Hydroxyl orientations in 2:1 phillosilicates. Clays Clay Miner 27: 213–223

Herrero CP, Sanz J (1991) Short-range order of the Si,Al distribution in layer silicates. J Phys Chem Sol 52: 1129–1135

Jackson RA, Catlow CRA (1988) Computer simulation studies on zeolite structures. Mol Simul 1: 207–224

Manceau A, Lanson B, Drits VA, Chateigner D, Gates WP, Wu J, Huo D, Stucki JW (2000) Oxidation–reduction mechanism of iron in dioctahedral smectites: I. Crystal chemistry of oxidized reference nontronites. Am Mineral 85: 133–152

McCarty DK, Reynolds RC Jr (1995) Rotationally disordered illite/smectite in paleozoic K-bentonites. Clays Clay Miner 43: 271–284

Post JE, Burnham CW (1986) Ionic modeling of mineral structures and energies in the electron gas approximation: TiO_2 polymorphs, quartz, forsterite, diopside. Am Mineral 71: 142–150

Sainz-Díaz CI, Timon V, Botella V, Hernández-Laguna A (2000) Isomorphous substitution effect on the vibration frequencies of hydroxyl groups in molecular cluster models of the clay octahedral sheet. Am Mineral 85: 1038–1045

Sainz-Díaz CI, Hernández-Laguna A, Dove MT (2001) Modelling of dioctahedral 2:1 phyllosilicates by means of transferable empirical potentials. Phys Chem Miner 28: 130–141

Sauer J, Ugliengo P, Garrone E, Saunders VR (1994) Theoretical study of van der Waals complexes at surface sites in comparison with the experiment. Chem Rev 94: 2095–2160

Schröder K-P, Sauer J, Leslie M, Catlow CRA, Thomas JM (1992) Bridging hydroxyl groups in zeolitic catalysts: a computer simulation of their structure, vibrational properties and acidity in protonated faujasites (H–Y zeolites). Chem Phys Lett 188: 320–325

Tsipursky SI, Drits VA (1984) The distribution of octahedral cations in the 2:1 layers of dioctahedral smectites studied by oblique-texture electron diffraction. Clay Miner 19: 177–193

Winkler B, Dove MT, Leslie M (1991) Static lattice energy minimization and lattice dynamics calculations on aluminosilicate minerals. Am Mineral 76: 313–331